PAGEOPH, Vol. 142, No. 3/4 (1994)

0033–4553/94/040419–27$1.50 + 0.20/0

Dynamic Faulting under Rate-dependent Friction

ALAIN COCHARD[1] and RAÚL MADARIAGA[1]

Abstract—We discuss the effects of rate-dependent friction on the propagation of seismic rupture on active faults. Several physicists using Burridge and Knopoff's box and spring model of faulting have proposed that fault complexity may arise from the spontaneous development of a self-similar stress distribution on the fault plane. If this model proves to be correct, it has important consequences for the origin of the complexity of seismic sources. In order to test these ideas on a more realistic earthquake model, we developed a new boundary integral equation method for studying rupture propagation along an antiplane fault in the presence of nonlinear rate-dependent friction. We study rupture dynamics of models with single and twin asperities. In our models, asperities are places on the fault with a higher value of prestress. Otherwise all fault parameters are homogeneous. We show that for models with such asperities, a slip velocity weakening friction leads to the propagation of supersonic healing phases and to the spontaneous arrest of fracture if the prestress outside the asperities is low enough. For models with asperities, we can also observe narrow slip velocity pulses, qualitatively similar to the so-called Heaton pulses observed in some earthquake accelerograms. We also observe a complex distribution of stress after the rupture that depends on details of the initial distribution of asperities and on the details of the friction law.

Key words: Seismicity, fracture, elastodynamics, friction, earthquakes, boundary integral equations.

1. Introduction

In the last 15 years, several alternative hypotheses have been discussed in the literature addressing the origin of earthquake complexity and, therefore, the radiation of seismic waves from complex events (KANAMORI and STEWART, 1978; DAS and AKI, 1977b; MADARIAGA, 1979, etc.). Two extreme views of this problem have been advanced. From the first viewpoint, complexity is due to permanent geometrical features on the fault surface, which control the initiation, arrest and radiation from seismic faults. Seismologists refer to them as barriers and asperities. In another approach, e.g., CARLSON and LANGER (1989), the complexity of faulting is considered as a dynamic feature of fault zones. Stress on the fault zone would constantly evolve, but would stay at a critical state such that complexities of all scales would be continuously created and destroyed. These two models have direct bearing on the generation of accelerograms, because radiation of high-frequency

[1] Département de Sismologie, Institut de Physique du Globe de Paris et Université Paris 7, 4, Place Jussieu (Tour 14–24), Boîte 89, 75252 PARIS CEDEX 05, France.

waves is the product of the interaction of an expanding rupture front with heterogeneities on the fault (MADARIAGA, 1983).

In general, seismic source complexity may be due either to heterogeneities in the state of stress of the fault, or to variations of strength. The latter is most probably due to the geometrical discontinuity of natural fault systems and may be considered as a permanent feature of faults—at least for time scales of less than a few thousand years. Stress heterogeneities, on the other hand, are a consequence of previous activity on the fault and may be dynamically controlled. Even though it is not always clearly stated in the literature, many authors do not necessarily consider barriers and asperities as permanent features on active faults. An extreme model of heterogeneity, that has become very popular in recent years, is the so-called characteristic earthquake model of SCHWARTZ and COPPERSMITH (1984). In this model, geometrical discontinuities on the fault persist for a very long time controlling the size of earthquakes. Although seismic activity in many subduction zones does not seem to agree with the simplest versions of the characteristic earthquake model (see, e.g. the seismicity of central Chile, KORRAT and MADARIAGA, 1986; COMPTE *et al.*, 1986), the relative role of permanent and transient heterogeneities on fault systems is presently unclear. The study of different models for the heterogeneity—geometric, static or dynamic control—is very difficult. Most of the crucial observations that would be needed to explore the origin of heterogeneity depend on the availability of geometrical information concerning the rupture process, on frictional behavior at high slip velocities, and on the details of the distribution of fault strength. Until such data are available, most of the research must be based upon careful numerical simulation using fracture models and friction laws that are as realistic as possible. This is the main goal of this paper.

2. Models of Source Heterogeneity

In this paper we study a model of seismic rupture in which we consider that earthquakes are due to the fast, catastrophic development of a frictional instability along a pre-existing fault surface. A fault is considered to be the result of numerous events upon which have taken place. These mature fault zones are the site of intense seismic activity with earthquakes of a wide spectrum of magnitudes or seismic moment occurring at any given site on these faults.

In a recent paper, CARLSON and LANGER (1989) (CL in the following) revitalized the block-and-spring model of BURRIDGE and KNOPOFF (1967) (B-K in the following). In most other studies of the B-K model—with a few exceptions like CAO and AKI (1986)—the frictional law of BRACE and BYERLY (1966) was applied. In this law, friction is assumed to be linearly proportional to the normal pressure across the fault, but to be independent of slip or slip velocity on the fault. Following BURRIDGE and KNOPOFF (1967), CARLSON and LANGER (1989) used a

simple rate-dependent frictional law in their simulations. Starting from a very small stress initial heterogeneity CL observed that heterogeneity developed in a natural way until it reached a self-similar distribution. Slip events (earthquakes) of all sizes were observed on the same stretch of the fault and they found that these events obeyed a Gutenberg-Richter law. CL attributed this behavior to the intrinsic instability of the rate-dependent friction.

In the B-K model each block obeys well-posed mechanical equations and reproduces, at least locally, the frictional interaction that is widely believed to be the cause of earthquakes. Unfortunately, this model has several limitations well-known to seismologists: it does not radiate seismic waves and it does not include long-range elastic forces. RICE (1993) has raised the even stronger objection, namely, that this model may be intrinsically discrete such that the observed heterogeneity may be due to inadequate sampling of the friction law on the fault.

In order to test the applicability of CL results to earthquakes it is clearly necessary to study a more realistic earthquake model, based on the elastodynamics of rupture propagation. As a first step in that direction, we present a study of the properties of an antiplane fracture model, employing a general rate-dependent model for friction. To our knowledge, the only previous work on the dynamic of faulting in a continuum with rate-dependent friction is that of OKUBO (1989) who used the friction law proposed by DIETERICH (1972). His results did not show any heterogeneity of the final stress. Our results are different: using the same models as OKUBO (1989) with the friction law used by CL, we will show that the final stress on the fault becomes heterogeneous.

3. A Shear-crack Model

We study the elastodynamic field due to a flat antiplane crack Γ that extends along the $z = 0$ line in a homogeneous linearly elastic medium of rigidity μ, density ρ and shear wave velocity $\beta = \sqrt{\mu/\rho}$ (Fig. 1). The only displacement component in this case is $u_y(x, z, t)$ that will be denoted simply u in the following, and the only nonzero elements of the stress tensor are $\sigma_{yx} = \mu\, \partial u/\partial x$ and $\sigma_{yz} = \mu\, \partial u/\partial z$.

The equation of motion is

$$\frac{1}{\beta^2}\frac{\partial^2 u}{\partial t^2} = \nabla^2 u. \tag{1}$$

The boundary conditions on the fault plane are

$$\begin{aligned} &\sigma_{yz}(x, t) = -T(x, t) \quad \text{on} \quad \Gamma \\ &\Delta u(x, t) = 0 \qquad\qquad\quad \text{on the complement of } \Gamma \end{aligned} \tag{2}$$

where the slip across the fault is defined as $\Delta u = u(x, 0^+, t) - u(x, 0^-, t)$, the traction change T across the fault being affected by a minus sign because the

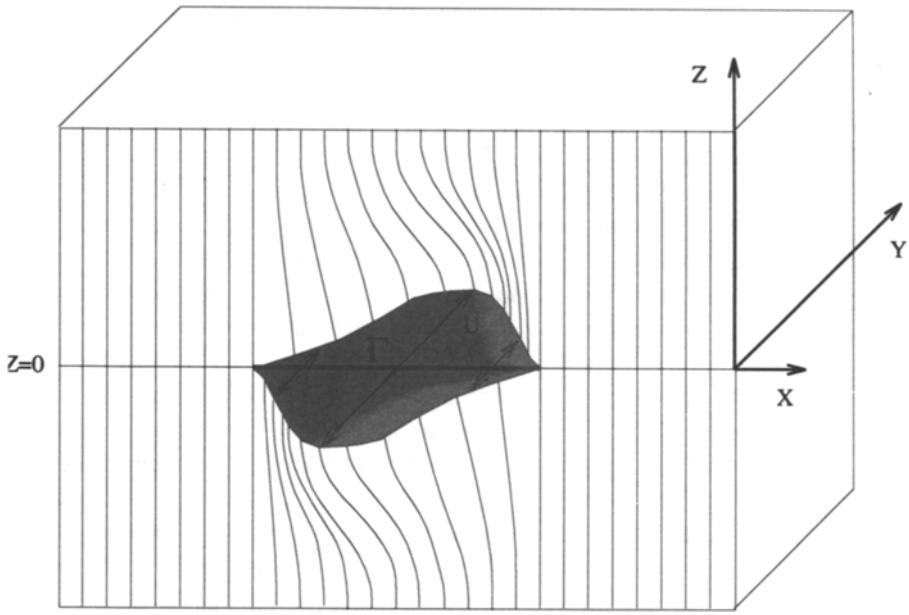

Figure 1
Geometry of the antiplane shear crack. The fault area is located on the $z = 0$ plane of an infinite, homogeneous, isotropic medium. The system is invariant with respect to translation along the Y axis. No opening of the crack is allowed. Slip u and discontinuity of slip are allowed along the Y direction. The fault can expand along the X axis.

normal to the upper half space ($z > 0$) points downwards. Usual radiation conditions are assumed at infinity.

Although the problem is extremely simplified, the mixed boundary value problem (1, 2) can be solved exactly only for very simple forms of the crack Γ and for special values of the traction change T in the cracked part of the interface. Here we are interested in studying the effect of friction so that the absolute traction T_{abs} is in fact a function of the slip velocity $\Delta\dot{u}$. The boundary value problem becomes nonlinear and it can only be solved by numerical methods.

We seek solutions of the problem (1, 2) by the boundary integral equation (BIE) method. This is relatively easy for the problem at hand because we know the Green function in closed form. We start from the classical Betti representation theorem. Displacement inside the elastic body is given by

$$u(x, z, t) = \int_{\Gamma} \int_{0}^{t} \Delta u(\xi, \tau) \Sigma(x, z, \xi, t - \tau)\, d\tau\, d\xi, \tag{3}$$

where $\Sigma = \mu\, \partial G/\partial z$ is the yz element of the stress tensor associated with the 2D Green function

$$G(x, z, \xi, t) = \frac{1}{2\pi\mu} \frac{H(t - r/\beta)}{\sqrt{t^2 - r^2/\beta^2}} \tag{4}$$

where $r = \sqrt{(x-\xi)^2 + z^2}$ and H is the Heaviside function. When $z \to 0$, (3) reduces to an identity, so that this version of the representation theorem does not lead to a useful BIE.

In order to get an integral equation we calculate first the change in the stress field σ_{yz} due to the slip Δu. Then we let $z \to 0$.

From (3) we get the integral equation:

$$T(x, t) = -\int_\Gamma \int_0^t \Delta u(\xi, \tau)\mu^2 \frac{\partial^2}{\partial z^2} G(x, 0, \xi, t-\tau)\, d\tau\, d\xi. \tag{5}$$

Replacing the two-dimensional Green's function in (5) we get finally

$$T(x, t) = -\frac{\mu}{2\pi\beta^2} \int_\Gamma \int_0^{\tau_m} \frac{\Delta u(\xi, \tau)}{[(t-\tau)^2 - (x-\xi)^2/\beta^2]^{3/2}}\, d\tau\, d\xi \tag{6}$$

where $\tau_m = \max(0, t - \|x - \xi\|/\beta)$. This appears to be a very simple integral equation, unfortunately, it cannot be used as it is because it is hyper-singular near the source point, when $\xi \to x$ and $\tau \to t$.

To obtain a proper integral equation we use the general method proposed by KOLLER *et al.* (1992). Assuming that Δu and its derivative with respect to x (the dislocation density) are continuous, we can transform (6) into the following regularized integral equation (i.e., an integral equation with an integrable kernel):

$$T(x, t) = -\frac{\mu}{2\pi} \int_\Gamma \int_0^{\tau_m} \left[\frac{t-\tau}{x-\xi} \frac{\partial}{\partial \xi} \Delta \dot{u}(\xi, \tau) + \frac{1}{\beta^2} \frac{\partial}{\partial \tau} \Delta \dot{u}(\xi, \tau) \mathscr{G}(t-\tau; x-\xi)\, d\tau\, d\xi \right] \tag{7}$$

where $\mathscr{G}(t-\tau; x-\xi) = ((t-\tau)^2 - (x-\xi)^2/\beta^2)^{-1/2}$, $\tau_m = \max(0, t - \|x-\xi\|/\beta)$ and $\Delta \dot{u}$ is the slip velocity. The domain of integration of equation (7) is shown in Figure 2. This form of the integral equation is particularly useful for setting up numerical methods for the solution of the boundary value problem.

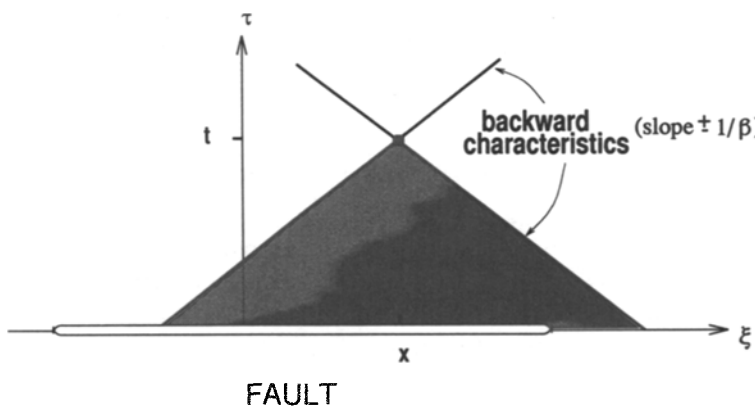

Figure 2
Domain of integration of the integral equation: a point can receive information of all the other points that lie inside the causality cone defined by the shear wave speed β.

Integral equation (7) is regular everywhere except near $\xi \to x$ where it must be interpreted in the usual sense of a Cauchy integral. Equation (7) has been regularized but is not symmetric. The first term relates stress on the boundary to the time and space derivative of the slip. In the parlance of dislocation theory, $\partial_\xi \, \Delta \dot{\mathbf{u}}$ can be simply written $\dot{\mathbf{b}}$ where $\mathbf{b}$ is the Burger's vector or dislocation density. The second term of this integral equation contains the second-order time derivative of slip. This term has a more complex structure: it contains the instantaneous response of a crack to stress change. This instantaneous response is associated with the radiation of a plane wave from the crack. The second term also contains a response to laterally heterogeneous slip functions such that it would be preferable to rewrite it in terms of some Burger's vector rate as the first term. In order to do this we must separate the instantaneous response from the BIE. This is a relatively difficult problem to solve in the space-time formulation. For this reason we prefer to introduce double Laplace transforms in space and time and we invert the Laplace transforms using the convolution theorem and Cagniard's method. This is done in Appendix 1. We obtain

$$T(x, t) = -\frac{\mu}{2\beta} \Delta \dot{u}(x, t) - \frac{\mu}{2\pi} \int_\Gamma \int_0^{\tau_m} \frac{\sqrt{(t-\tau)^2 - (x-\xi)^2/\beta^2}}{(t-\tau)(x-\xi)} \frac{\partial}{\partial \xi} \Delta \dot{u}(\xi, \tau) \, d\tau \, d\xi. \quad (8)$$

With this formulation, we immediately see that an instantaneous traction change produces a Heaviside like change in slip velocity.

Similar to integral equation (7), integral equation (8) is regular everywhere except near $\xi \to x$ where it must be interpreted in the usual sense of a Cauchy integral. This Cauchy like singularity is associated with the static field of a dislocation. The second term in (8) is the effect of diffraction of waves by the dislocation distribution on the fault. This term contains both long-range elastic interactions—inversely proportional to $x - \xi$—and wave interactions due to the wavefront singularities that propagate the shear wave speed (β) along the fault.

4. *Rate-dependent Friction*

With the previously mentioned exception of the paper by OKUBO (1989) and the approximate discussion in HEATON (1990), all previous work on fracture simulation has been accomplished either with a constant kinematic friction or a slip weakening friction law. Recently, based on experimental data, several authors (e.g., DIETERICH, 1972; RICE and RUINA, 1983; GU *et al.* 1984) have proposed that friction is a nonlinear function of slip velocity and a number of hidden thermodynamic variables that describe the state of the fault at the time of the earthquake. This was the friction law used by OKUBO (1989).

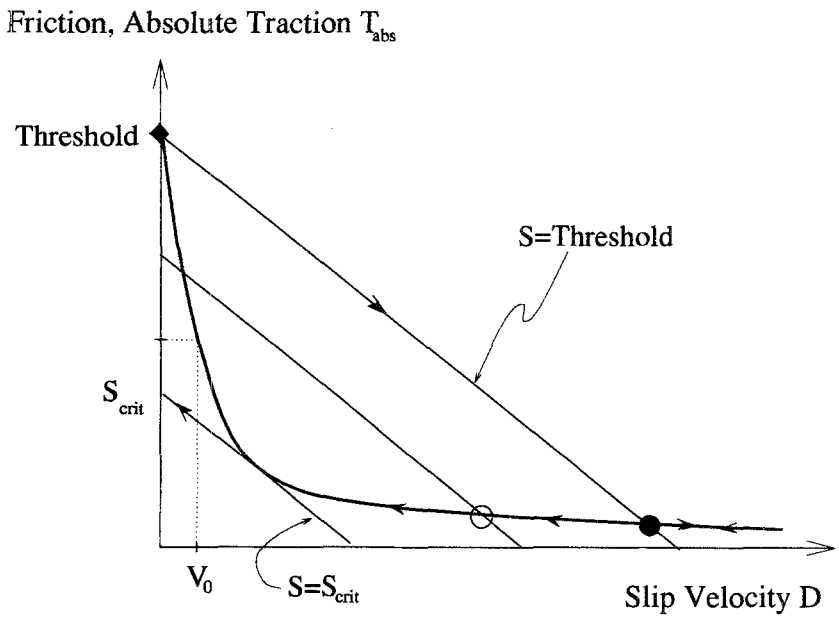

Figure 3
Slip velocity weakening friction law and the mechanism of instability for one element of the crack line. There is a jump in slip velocity and absolute traction for this element at the beginning and at the end of slip along the radiation damping lines.

In their study of the B-K model, CARLSON and LANGER (1989) on the other hand used a simplified velocity-dependent friction law initially proposed by BURRIDGE and KNOPOFF (1967). This law shown in Figure 3 contains no internal state variable nor scale length:

$$T_{abs}(\Delta\dot{u}) = T_{thres}\frac{V_0}{V_0 + \Delta\dot{u}} \tag{9}$$

where T_{abs} is the absolute traction, $\Delta\dot{u}$ is the slip velocity, V_0 is a reference velocity that determines the rate of slip velocity weakening in the model and T_{thres} is the traction threshold or equivalently the maximum traction drop, reached when the slip velocity is very large.

This friction law is clearly unstable because the traction T_{abs} decreases with increasing slip velocity. It is very unstable for low values of slip rate; for larger values of slip velocity, friction drop reaches a finite limit and instability decreases.

5. Numerical Solution of the Fault Model

A general method for discretizing equation (7) was discussed by KOLLER *et al.* (1992). Their technique leads to a system of implicit equations for the determina-

tion of slip on the fault. This method cannot be used without major changes required to solve the nonlinear rate-dependent friction (9). For our purposes we introduce the following extremely simple discretization of the slip-velocity field inspired from the displacement discontinuity method:

$$\Delta\dot{u}(x, t) = \sum_{j,m} D_{j,m}\, d(x, t; x_j, t_m) \tag{10}$$

where $d(x, t; x_j, t_m)$ is a simple box-car function defined in the following fashion:

$$\begin{aligned} &d(x, t; x_j, t_m) = 1 \quad \text{if} \quad x_j \le x < x_{j+1} \quad \text{and} \quad t_m \le t_m \le t < t_{m+1} \\ &d(x, t; x_j, t_m) = 0 \quad \text{otherwise.} \end{aligned} \tag{11}$$

Noticing that d can be written in the following compact form

$$\begin{aligned} d(x, t; x_j, t_m) = {} & H(x - x_j)H(t - t_m) - H(x - x_{j+1})H(t - t_m) \\ & - H(x - x_j)H(t - t_{m+1}) + H(x - x_{j+1})H(t - t_{m+1}), \end{aligned} \tag{12}$$

and inserting the discretized slip-velocity field (10) in the integral equation (8) we obtain

$$T(x, t) = -\frac{\mu}{2\beta} \sum_{j,m} D_{j,m} K(x, t; x_j, t_m) \tag{13}$$

where

$$\begin{aligned} K(x, t; x_j, t_m) = {} & I(x - x_j, t - t_m) - I(x - x_{j+1}, t - t_m) \\ & - I(x - x_j, t - t_{m+1}) + I(x - x_{j+1}, t - t_{m+1}) \end{aligned} \tag{14}$$

with

$$\begin{aligned} I(x, t) = {} & H(t)H(x) \\ & + \frac{1}{\pi} H(t - \|x\|/\beta) \left[\frac{\sqrt{1 - (x/\beta t)^2}}{x/(\beta t)} - \sin^{-1}\left(\sqrt{1 - (x/\beta t)^2}\right) \operatorname{sign}(x) \right]. \end{aligned} \tag{15}$$

We can reduce the integral equation (13) to a discrete problem by collocating the equation at a series of knots located inside each boundary element. These collocation points are defined by the coordinates $x_i + \varepsilon_x\, \Delta x$ and times $t_n + \varepsilon_t\, \Delta t$ with $\varepsilon_x, \varepsilon_t \in [0, 1]$. Writing

$$T_{i,n} = T(x_i + \varepsilon_x\, \Delta x, t_n + \varepsilon_t\, \Delta t) \tag{16}$$

and noticing by straightforward analysis of expression (14) that K can be written in the simpler form $K(x, t; x_j, t_m) = K(x - x_j, t - t_m)$, we derive the linear system

$$T_{i,n} = -\frac{\mu}{2\beta} \left[D_{i,n} + \sum_{\substack{j \\ m \le n-1}} D_{j,m} K_{i-j,n-m} \right] \tag{17}$$

where

$$K_{i-j,n-m} = K(x_i - x_j + \varepsilon_x \Delta x,\ t_n - t_m + \varepsilon_t \Delta t). \tag{18}$$

Because $K_{k,l}$ must be equal to $K_{-k,l}$ (by symmetry), ε_x must be equal to $\frac{1}{2}$. We found that $\varepsilon_t = 1$ produces the best results so this is the value that is used in the numerical simulations.

5.1. *Solution of the Integral Equation*

In order to solve the integral equation at any given time step n, we must distinguish between boundary elements that are in the process of slipping for which we want to calculate the slip rate $D_{i,n}$, from boundary elements that are locked, for which either the rupture front has not yet arrived or that have already slid and healed.

Knowing that $T_{i,n}$ is the traction change, we can rewrite equation (17) in the following way:

$$T_{\mathrm{abs}_{i,n}} = -\frac{\mu}{2\beta} D_{i,n} + T_{0_i} - \frac{\mu}{2\beta} \sum_{m=0}^{n-1} \sum_j D_{j,m} K_{i-j,n-m} \tag{19}$$

where T_{0_i} is the initial traction of element i.

The solution of equation (19) for a boundary element i that is slipping at time n is

$$D_{i,n} = \frac{2\beta}{\mu} [T_{\mathrm{abs}_{i,n}} - T_{0_{i,n}}] + \sum_{m=0}^{n-1} \sum_j D_{j,m} K_{i-j,n-m} \tag{20}$$

where $T_{\mathrm{abs}_{i,n}}$, the absolute traction, is obtained from the friction law (9) in the crack:

$$T_{\mathrm{abs}_{i,n}}(D_{i,n}) = T_{\mathrm{thres}_i} \frac{V_0}{V_0 + D_{i,n}} \tag{21}$$

Equations (20, 21) must be solved simultaneously for $T_{\mathrm{abs}_{i,n}}$ and $D_{i,n}$.

For an element i that was locked at time $n-1$, we decide that it is going to slip at time n if its absolute traction assuming that it remains locked becomes greater than the friction threshold i.e., if

$$T_{0_i} - \frac{\mu}{2\beta} \sum_{m=0}^{n-1} \sum_j D_{j,m} K_{i-j,n-m} \geq T_{\mathrm{thres}_i}. \tag{22}$$

We are aware of the fact that this absolute rupture criterion is not a correct rupture criterion. But as we are only interested for the present paper in qualitative results on the effect of rate-dependent friction, we use it (as is often done), for the sake of simplicity.

Finally, if it is no longer possible to solve (20, 21), we decide that $D_{i,n}$ becomes 0; this arrest criterion will become clear in the next section.

Thus boundary conditions are imposed very simply without recomputing the complete solution at the current time. This is the main advantage of the explicit formulation with respect to the implicit boundary element method developed by KOLLER *et al.* (1992).

5.2. Instability of Crack Slip for Rate-dependent Friction

The role of frictional instability in the crack model can be easily understood analyzing the discretized integral equation (19). Introducing a simplified notation, we rewrite it in the form

$$T_{\mathrm{abs}_{i,n}} = -\frac{\mu}{2\beta} D_{i,n} + S_{i,n} \tag{23}$$

with $S_{i,n} = T_{0_i} - \mu/2\beta \sum_{m=0}^{n-1} \sum_j D_{j,m} K_{i-j,n-m}$.

Equation (23) is a nonlinear algebraic equation for the slip rate $D_{i,n}$ on the fault, whose solution is in fact controlled by the value of $S_{i,n}$. The solution of the equation at different instants of the slip cycle may be better discussed by referring to Figure 3 which shows the friction-slip velocity phase space. We can notice that, in this phase space, equation (23) represents a family of straight lines with slope $-\mu/2\beta$. From a geometrical point of view, the solution of the integral equation (23) at a given point i with the rate-dependent friction (21) can be understood as being determined by the intersection of one of these straight lines with the friction curve. Slip on the fault starts when $D = 0$ and T_{abs} reaches the friction threshold. This is indicated by the diamond in Figure 3 and corresponds to $S = \textit{threshold}$. At this time, element i is in an unstable equilibrium and the traction suddenly drops to a value determined by the intersection of the straight line labelled $S = \textit{threshold}$ with the friction law. This is indicated by the dot in the same figure. For later times, element i receives information from the other elements of the fault such that the value of S is modified, resulting in a translation of the straight line parallel to itself and consequently to a variation of D along the friction curve (cf. circle in Figure 3). There are actually two intersections between the straight line and the friction curve but the one of interest to us is the one with lower stress. Eventually slip velocity decreases until S reaches a critical value S_{crit} such that the straight line labelled S_{crit} is tangent to the friction law. At this time, the crack element i is at a bifurcation point and, as a result, $D_{i,n}$ drops instantaneously to 0 and that fault element locks. At the same time, the absolute traction $T_{i,n}$ increases to $S_{\mathrm{crit}_{i,n}}$.

In the course of slip, a point on the fault schematically follows the trajectory indicated by the arrows in the phase space of friction and slip rate. Let us note that more complex nonlocal frictional laws may require some substantial change in the method of solution.

Thus cracks under rate-dependent friction are unstable, traction on the fault jumps abruptly at both the beginning and the end of slip. This sudden stress drop and stress locking is quite similar to the partial stress drop proposed by BRUNE (1970). Recently HEATON (1990) proposed that the source time history of several earthquakes determined from the inversion of near-field accelerograms indicated that the rise time of these events was very short. He proposed that rate-dependent friction was the cause of this observation. We will return to this in the discussion.

5.3. *Numerical Implementation in the Connection Machine*

We must solve the discretized integral equation (19):

$$T_{\mathrm{abs}_{i,n}} = -\frac{\mu}{2\beta} D_{i,n} + T_{0_i} - \frac{\mu}{2\beta} \sum_{m=0}^{n-1} \sum_{j} D_{i,n} K_{i-j,n-m}. \tag{24}$$

The computation starts from an initial state of absolute traction T_{0_i} along the x axis at time <0. Thus it is necessary for at least one element to be at the threshold so as to initiate the movement. From this state of traction, we immediately deduce the velocity D and traction T_{abs} for $n = 0$. Then we have to compute simultaneously $T_{\mathrm{abs}_{i,n}}$ and $D_{i,n}$ step by step for times $n \geq 1$. It consists mainly of computing the double sum over space and time $\Sigma_{m=0}^{n-1} \Sigma_j D_{j,m} K_{i-j,n-m}$. This is a discrete convolution over space and time of the slip velocity field D by the kernel K which is computed with Fast Fourier Transforms using the massively parallel super computer of Institut de Physique du Globe de Paris: the connection machine CM-5. Each of the three simulations presented in this paper took about 3 minutes cpu time on the CM-5 with 128 processors.

Our numerical computations are made using the following nondimensional quantities:

$$T'_{\mathrm{abs}} = \frac{2T_{\mathrm{abs}}}{\mu}, \quad D' = \frac{D}{\beta}, \quad x' = \frac{x}{\Delta x}, \quad t' = \frac{t\beta}{\Delta x}, \tag{25}$$

where Δx is the length of a boundary element $x_{i+1} - x_i$. Finally we have to fix the value of $\beta\, \Delta t/\Delta x$, Δt being the time step $t_{n+1} - t_n$. This value is fixed to 1/2, as in KOLLER *et al.* (1992) for the computations presented in this paper.

We refer the reader to our previous papers (MADARIAGA and COCHARD, 1992 and KOLLER *et al.*, 1992) for an extensive check of the validity of the numerical method. We present in Appendix 2 one comparison with the analytical result obtained by BURRIDGE (1969).

6. *Numerical Results: Single and Twin Asperity Models*

Following the work of OKUBO (1989), we shall illustrate numerically the effect of rate-dependent friction when the initial states of stress along the fault plane (x

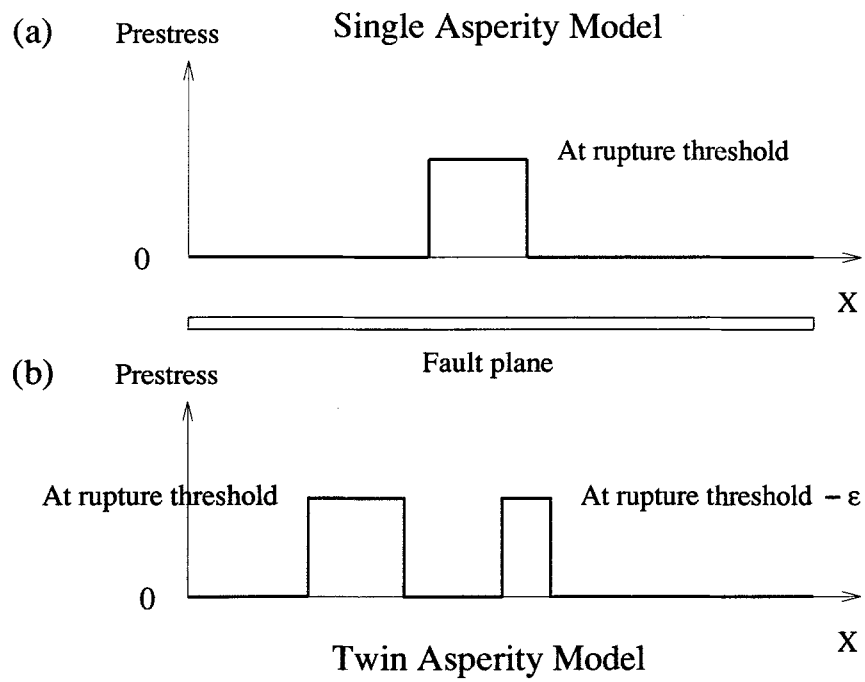

Figure 4
Initial states of stress for the numerical simulations presented in this paper. (a) One asperity. (b) Two asperities. The stress outside the asperities is 0.

axis) are those shown in Figure 4. Figure 4a represents a single asperity: a given length of the fault axis is at the rupture threshold at time 0 and the stress outside this patch is 0. In Figure 4b, we have two asperities: the first one is at rupture threshold and the second one is almost at rupture threshold so it is ready to break.

For the simulations presented in this paper, the single asperity of Figure 4a is 100 elements large, the two asperities of Figure 4b are 100 and 50 elements large, separated by 100 elements; for clarity of the figures, only one line in ten is presented in the space-time plots to follow. In all the computations, the nondimensional threshold $2T_{\text{thres}}/\mu$ was fixed to 5.

Figures 5 and 6 represent the evolution of slip velocity along the fault for the single asperity model when friction is not rate-dependent i.e., when $v_0 = 0$, $v_0 = V_0/\beta$ being the nondimensional parameter that determines the amount of slip-velocity weakening in the friction law (21). The rupture threshold is assumed to be uniform along the section of the fault plane that is allowed to break. Outside this section, the threshold is assumed to be infinity, yielding an effectively unbreakable barrier. After the initial crack appears, stress concentrations develop near the edges of the crack until traction across the fault reaches the friction threshold. At that point rupture begins to grow with a velocity that becomes rapidly comparable to that of

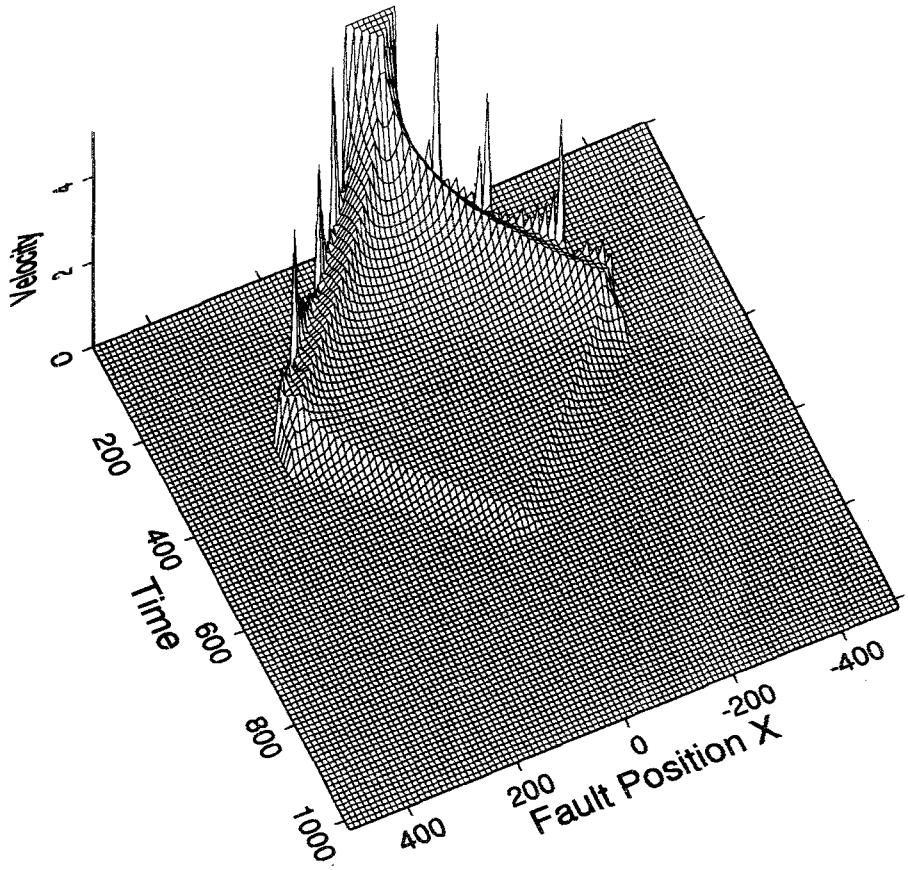

Figure 5
The slip-velocity field for the single asperity model with constant friction ($v_0 = 0$). Rupture fronts are stopped only when encountering the barriers.

shear waves in the material surrounding the fault. Rupture continues until the rupture fronts reach the barriers. Stopping phases then are emitted and propagate backward to the center of the fault. The slip velocity of an element i inside the fault decreases slowly until the arrival of a stopping phase. It then decreases rapidly to 0. Therefore in the case of classical (rate-independent) friction, the global arrest of rupture is due to the stopping phases emanating from the edges of the fault.

We see in Figure 6 that the stress after the rupture is very smooth inside the fault. It is slightly less than 0 due to the classical overshoot.

We now present numerical solutions for the same asperity of Figure 4a but with a small amount of rate-dependence $v_0 = 7 \times 10^{-2}$. The situation is quite different for the slip velocity evolution shown in Figure 7 (note the change in time scale). Because of the healing mechanism due to the instability of the friction law described

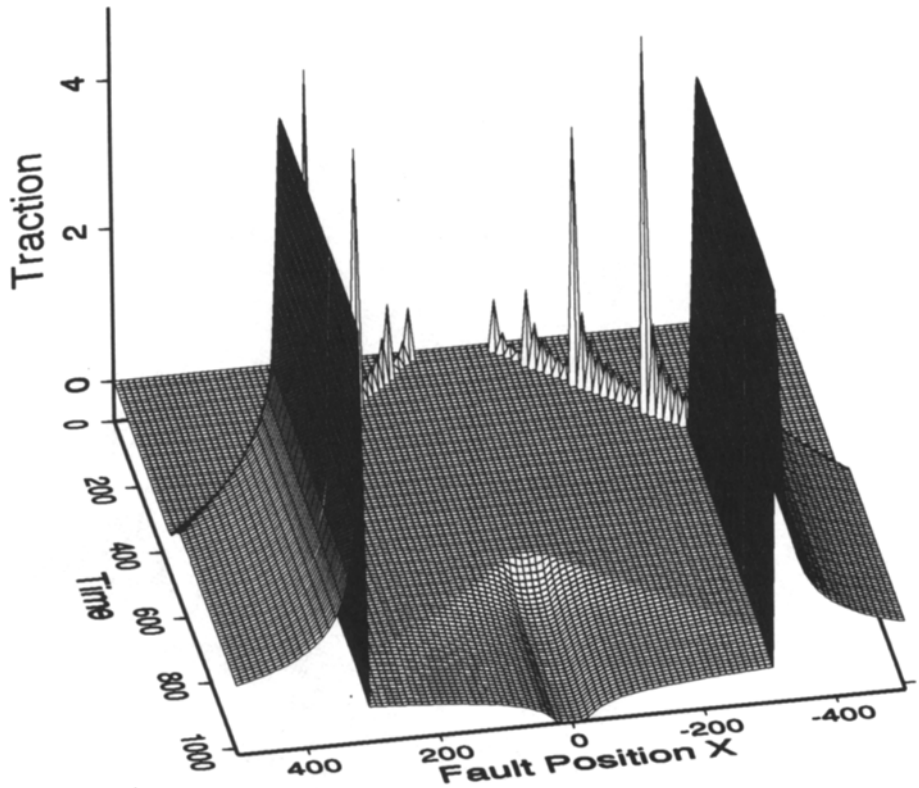

Figure 6
The stress field for the single asperity model with constant friction ($v_0 = 0$). Stress inside the fault is very smooth at the end of the rupture.

in Figure 3, an element inside the fault locks well before the arrival of the rupture front at the barriers. This behavior is quite like the self-healing pulses that HEATON (1990) reported to have been observed for several recent earthquakes modelled from near-field data.

The situation is also quite different for the stress evolution shown in Figure 8. When an element inside the fault locks, its traction jumps as shown in Figure 3. Then it receives information from other elements of the fault that are still moving: its traction increases and the earlier an element locks, the higher its traction is at the end of the global movement. As a consequence, the stress is higher at the center of the fault. On the contrary, we see that where the pulses stop, the traction decreases: this is classical overshoot, equivalent to what was observed in Figure 6 with rate-independent friction. In his paper, OKUBO (1989) found a similar result for the evolution of slip velocity for a model with a single asperity. On the other hand, he found that the final stress inside the broken patch is very close to 0. This

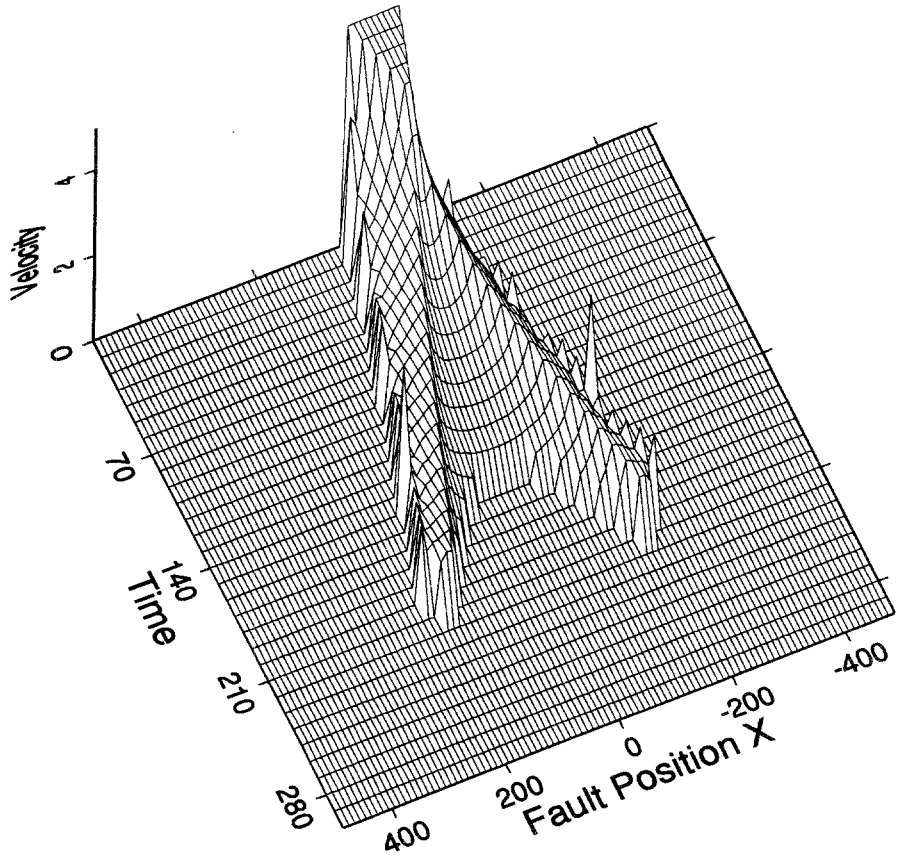

Figure 7
The slip-velocity field for the single asperity model with rate-dependent friction ($v_0 = 7 \times 10^{-2}$). Rupture stops spontaneously before reaching the barriers.

discrepancy is probably due to the difference between the friction laws used in the two cases: he used DIETERICH's (1972) rate-dependent friction law with high velocity cutoffs so that it is actually rate-independent at high slip velocities.

The evolution of slip velocity and traction for the twin asperity model (Figure 4b) in the presence of rate-dependent friction ($v_0 = 4.5 \times 10^{-2}$) is shown in Figures 9 and 10, respectively.

The first asperity, at rupture threshold, breaks at time 0 and the second one, almost at rupture threshold, is triggered by the arrival of the rupture front originating from the first one. As in the case of the single asperity model with rate-dependent friction, the global arrest of movement is spontaneous and due to the friction law. But due to the interference between the two asperities, the system can spontaneously develop a very important stress heterogeneity. Indeed, the corresponding plot with $v_0 = 0$ (not shown here) exhibits a very smooth final stress as in Figure 6.

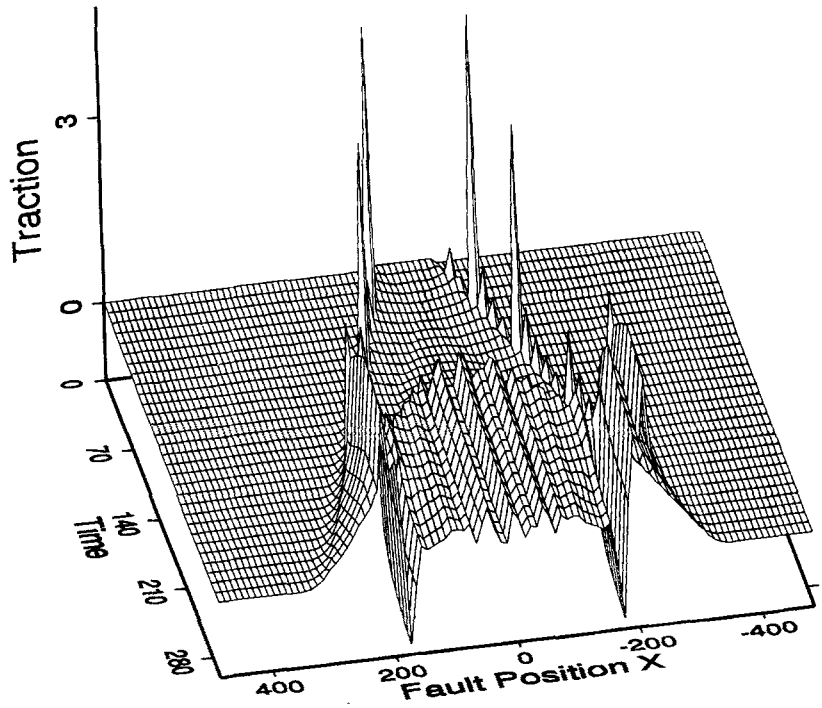

Figure 8
The stress field for the single asperity model with rate-dependent friction ($v_0 = 7 \times 10^{-2}$). Stress inside the fault is higher at the center and lower at the extremities of the pulses.

In order to verify the numerical precision of our solution, we would have preferred to compare the solution of Figures 9 and 10 with those obtained for different grid sizes. Unfortunately, this is not possible with the simple rupture criterion used here because, as is well-known, the amplitude of the traction just in front of the crack tip depends on the grid size (see for example DAS and AKI, 1977a), therefore the rupture history determined numerically will be very different. This problem was discussed in detail by KOLLER *et al.* (1992). Instead of this test, we can compare the solutions obtained with different grid sizes in the case of propagation with kinematically imposed rupture velocity. This is done in Appendix 2 and illustrates that the numerical solutions converge when we increase the number of grid points. We also discovered that numerical noise, due to the sudden locking of slip in the fault, decreases with the use of the finer grid. Convergence between the solutions obtained with different grid sizes for spontaneous propagation is diminished compared to the one observed in Figures 13 and 14 (see Appendix) because our model is of course "inherently discrete" in the sense given by RICE (1993). This is due to the lack of intrinsic length scale in the friction law (9). However, the main difficulties with the lack of length scale are that rupture velocity depends on the

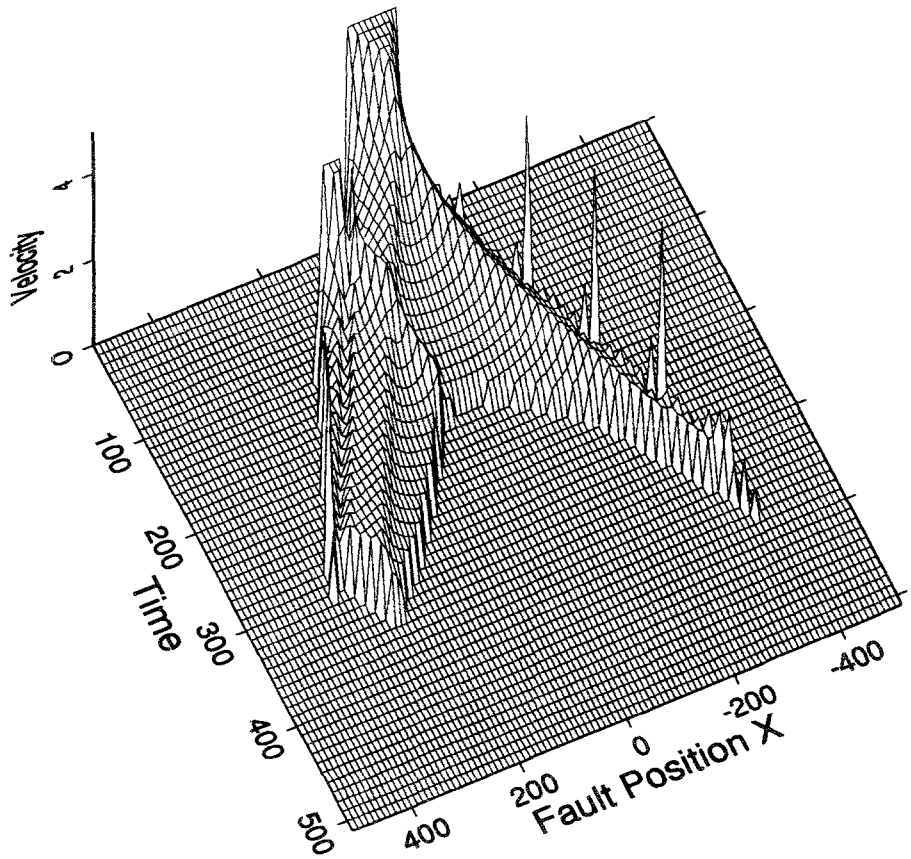

Figure 9
The slip-velocity field for the twin asperity model with rate-dependent friction ($v_0 = 4.5 \times 10^{-2}$).

grid, not that the stress field inside the fault would become smoother as proposed by RICE. Although we are convinced that a proper treatment of the rupture front would not qualitatively change the results presented in this paper, we will delay further discussion to a forthcoming paper in which we discuss analytical solutions for some simple fracture problems.

7. Discussion and Conclusions

We have developed a new Boundary Integral Equation Method to study antiplane dynamic faulting under rate-dependent friction.

From the solution of a model of faulting with a single initial stress asperity, we conclude that faulting under rate-dependent friction presents a number of fundamental differences with respect to KOSTROV's (1964, 1966) classical model of the

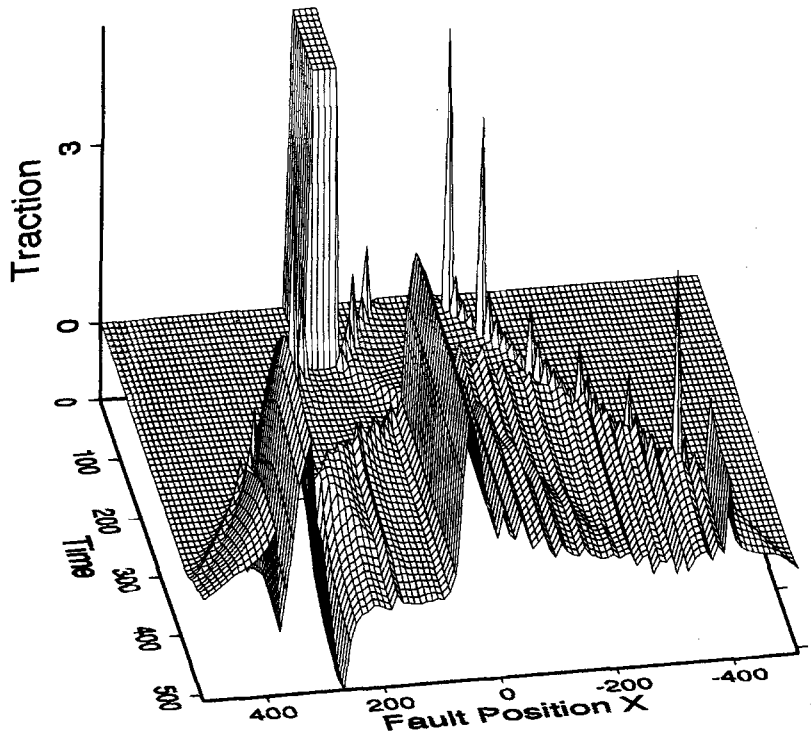

Figure 10
The stress field for the twin asperity model with rate-dependent friction ($v_0 = 4.5 \times 10^{-2}$). Stress inside the fault is very heterogeneous at the end of the rupture.

propagation of a simple crack under constant friction. The main new result is that rate-dependent friction makes fault healing unstable, thus slip velocity drops abruptly to zero inside the crack before the arrival of any stopping phase issued from the edges of the fault. Fault healing spreads from the center of the fault forming a "healing phase," the hyperbolic like curve where the slip velocity jumps to zero in Fig. 7. This phase propagates bilaterally at supersonic speed and finally draws even with the rupture front. Thus the whole rupture process may stop spontaneously before the rupture has had the time to reach the edges of the fault.

From the solution of the slightly more complex case of two interacting stress asperities, we find that stress heterogeneity may be spontaneously maintained on the fault plane. This is due to the instability of healing previously mentioned. This result is different from that of OKUBO (1989) who discovered in his simulations that, both for single and twin asperities, the state of stress inside the crack was invariably smoother and quite different from that of Figures 10 and 14. We believe that this is due to the use of the DIETERICH (1972) friction law, which is rate-dependent at very high slip velocities. This point will be further discussed in future work.

We must emphasize that our fault model contains no material heterogeneities. The rupture threshold is homogeneous along the fault axis (except at the ends of the fault which in fact play no part in the rupture history when the friction is rate-dependent) and so are the characteristics of the friction law. What we call an asperity is not a fault patch with a higher rupture threshold as is sometimes assumed, it is just an area where the *initial stress* is high compared with the surroundings. Presumably, this stress heterogeneity remains from a previous rupture event. It is clear that, had we included heterogeneities of the rupture threshold, we could have also observed short rise times and heterogeneous distributions of traction after the rupture as DAS and KOSTROV (1988) did.

It is beyond the scope of the two-dimensional model we used here to quantitatively compare the consequences of our model (short rise times) to real data. This will only be possible once we are able to solve for three-dimensional models. However, our numerical simulations are in qualitative agreement with Heaton's observation of short slip velocity pulses. He attributed this to the nonlinear rate dependence of friction: as slip velocity decreases, stress increases, driving the slip velocity deeper. While this is exactly what happens in our models, we still need a mechanism which makes the slip velocity decrease fast enough to produce short velocity pulses. In our models, this mechanism is actually provided by the asperities. As discussed above, in the single asperity model of Figure 4, slip velocity *naturally* decreases even with the classical friction law and the rate of this decrease depends on the value of the prestress outside the asperity: the more this prestress is removed far from the rupture threshold (closer to zero), the more rapidly slip velocity decreases. Consequently, with a rate-dependent friction law, the rise time depends on both the amount of rate dependence of friction, and on the difference between the prestress inside and outside the asperity. For example, one can have a relatively high rate dependence in the friction law, and yet be unable to induce the early arrest of slip if the prestress outside the asperity is not low enough. We will quantify these effects in a subsequent paper with the aid of analytical solutions. Simply stated: if the value of the prestress outside the asperity is low enough, and if the rate dependence of the friction law is high enough, then a short rise-time "healing phase" will appear and the rupture front will be stopped by the arrival of this "healing phase" (spontaneous arrest of the whole rupture).

The next step to be performed would be the computation of several cycles of events. The final state of stress of a given cycle would serve as the initial state of the following one (uniformly increased such that one element reaches the threshold, simulating some loading mechanism). The question is: will the stress distribution become spontaneously heterogeneous as in the box spring models of Carlson and Langer? In order to accomplish this, we must introduce a realistic rupture criterion instead of the numerical rupture criterion that we used in this paper.

Appendix 1: Derivation of the Integral Equation

Let us define the double Laplace transform of a function $f(x, t)$ of position x along the fault plane and time t by

$$\tilde{\bar{f}}(p, s) = \int_0^\infty \int_{-\infty}^\infty f(x, t)\, e^{-s(t-px)}\, dx\, dt \tag{26}$$

where $f(x, t) = 0$ for $t < 0$, and its inverse

$$f(x, t) = \frac{1}{2\pi i} \int_{C_s} \frac{1}{2\pi i} \int_{C_p} \tilde{\bar{f}}(p, s)\, e^{s(t-px)} s\, dp\, ds. \tag{27}$$

The transform over time—indicated by an overbar—is a one-sided Laplace transform; the inversion contour for this transform C_s is the customary Bromwich contour in the complex-s plane such that all singularities are to the left of the contour (see Fig. 11). Thus for negative t we can close the contour around positive real s so that $f(t) = 0$ for $t < 0$. The space transform, indicated by a tilde, is a two-sided Laplace transform. The inversion contour has to be placed in the complex-p plane such that the function $f(x)$ has the correct limit behavior at $\pm\infty$.

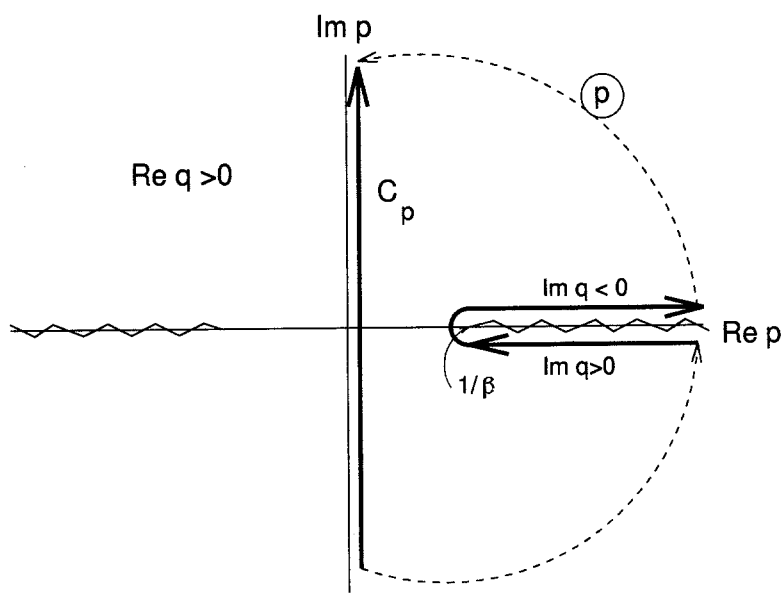

Figure 11
The complex-p plane for the inversion of Laplace transforms by Cagniard-de Hoop.

Let us write a few properties of the Laplace transform pairs (26) and (27) that we need in the following:

- time derivative $\partial_t f(t, x) \overset{\mathscr{L}}{\rightarrow} s\tilde{\tilde{f}}(p, s)$
- space derivative $\partial_x f(t, x) \overset{\mathscr{L}}{\rightarrow} -sp\tilde{\tilde{f}}(p, s)$
- time-space convolution $\int_{-\infty}^{\infty} \int_0^t f(\tau, \xi) g(t-\tau, x-\xi)\, d\tau\, d\xi \overset{\mathscr{L}}{\rightarrow} \tilde{\tilde{f}}\tilde{\tilde{g}}.$

Let us start again from expression (5)

$$T(x, t) = -\mu \int_\Gamma \int_0^t \Delta u(\xi, \tau) \frac{\partial^2}{\partial z^2} \mu G(x, 0, \xi, t-\tau)\, d\tau\, d\xi. \tag{28}$$

This a convolution between the double derivative of the Green function with respect to z and the slip function Δu. Its double Laplace transform can be evaluated using the transform of a convolution listed above and knowing the time-space Laplace transform $\tilde{\tilde{G}}$ of the Green function G given in equation (4):

$$\tilde{\tilde{G}}(p, z, s) = \frac{1}{2\mu} \frac{1}{sq} e^{-sqz}. \tag{29}$$

This result can be found with other notations on page 227, equation (6.44) of AKI and RICHARDS (1980). It is valid for $z > 0$. The sign of the square root should be taken so that $\mathrm{Re}\, q > 0$ in the upper Riemann sheet of q. Consequently the double Laplace transform of equation (28) is given by:

$$\tilde{\tilde{T}}(p, s) = -\frac{\mu}{2} \Delta\tilde{\tilde{u}}(p, s) sq. \tag{30}$$

Then we rewrite (30) in the form:

$$\tilde{\tilde{T}}(p, s) = -\frac{\mu}{2\beta} s\Delta\tilde{\tilde{u}}(p, s) - \frac{\mu}{2} [-s^2 p\, \Delta\tilde{\tilde{u}}(p, s)] \frac{1/\beta - q}{sp}. \tag{31}$$

This rather complex way of rewriting (30) is adopted so that the time and space derivative of $-s^2 p\, \Delta\tilde{\tilde{u}}$ appears in the integral equation instead of the slip function itself.

The last term has been separated from the first one in order to cancel the pole at the origin of the complex-p plane that would otherwise be produced by the factor p in the denominator of the first term in (31). Defining the operator

$$\tilde{\tilde{\mathcal{O}}}(p, s) = \frac{1/\beta - q}{sp}, \tag{32}$$

the new expression for the boundary integral equation (31) in the physical domain becomes:

$$T(x, t) = -\frac{\mu}{2\beta} \Delta\dot{u}(x, t) - \frac{\mu}{2} \int_\Gamma \int_0^t \mathcal{O}(x-\xi, t-\tau) \frac{\partial}{\partial \xi} \Delta\dot{u}(\xi, \tau)\, d\tau\, d\xi \tag{33}$$

where we used some of the standard Laplace transforms listed above. The instantaneous response relating stress and slip velocity is clearly separated in this integral equation. The only problem remaining is to compute the inverse transform of $\tilde{\bar{\mathcal{O}}}$, but this is very easy using the Cagniard-de Hoop method; we have:

$$\bar{\mathcal{O}}(x, s) = \frac{1}{2\pi i} \int_{C_p} \frac{1/\beta - q}{p} e^{-spx} \, dp. \tag{34}$$

The contour C_p on the complex-p plane is shown in Figure 11 where we also show the location of the branch cuts of q taken from the branch points at $p = \pm\beta^{-1}$ to infinity along the real p axis. The integral over p can be evaluated by deforming the contour of integration and folding it over the branch cuts. For $x > 0$ the contour is closed at $\mathrm{Re}\, p \to \infty$, and on the other side for $x < 0$. For positive x, we deform the integration contour along the branch cut located along the ositive Re p axis (see Figure 11). Taking into account that $\mathrm{Im}\, q < 0$ above the cut and $\mathrm{Im}\, q > 0$ below the cut, we derive

$$\begin{aligned} 1/\beta - q &= 1/\beta + i|q| \quad \text{above the branch cut} \\ 1/\beta - q &= 1/\beta - i|q| \quad \text{below the branch cut.} \end{aligned} \tag{35}$$

Summing the contour integrals above and below the branch cut, the term proportional to $1/\beta$ is continuous and does not contribute to the integral so that we are left with the simple expression

$$\bar{\mathcal{O}}(x, s) = \frac{1}{\pi} \int_{1/\beta}^{\infty} \frac{|q|}{p} e^{-spx} \, dp \tag{36}$$

where $|q| = \sqrt{p^2 - 1/\beta^2}$. Finally using the variable transformation $t = px$, we get

$$\bar{\mathcal{O}}(x, s) = \frac{1}{\pi} \int_{1/\beta}^{\infty} \frac{\sqrt{t^2 - x^2/\beta^2}}{tx} e^{-st} \, dt. \tag{37}$$

From this and a corresponding expression for negative x, we obtain

$$\mathcal{O}(x, t) = \frac{1}{\pi} \frac{\sqrt{t^2 - x^2/\beta^2}}{tx} H(t - |x|/B). \tag{38}$$

Inserting this into the integral equation (33) we finally get the BIE (8) that we wanted to obtain.

Appendix 2: Accuracy of the Numerical Method

Instantaneous Fault: Comparison with Analytical Results

BURRIDGE (1969) found an analytical solution for the slip velocity of an instantaneous antiplane fault without friction. The fault appears instantaneously

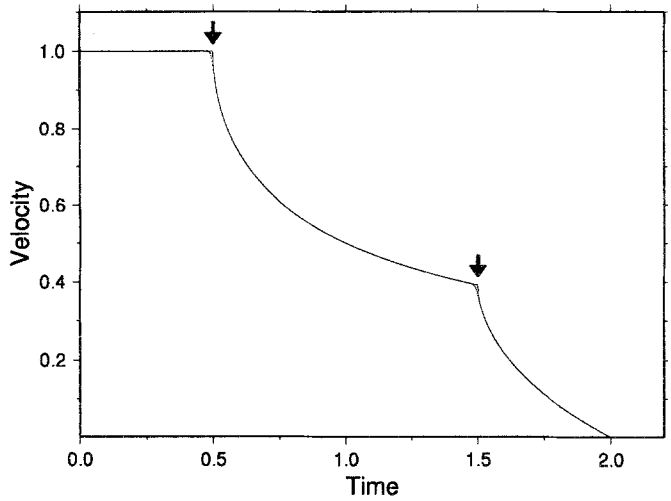

Figure 12

Analytical (full line) and numerical solution (dotted line) for the 256-th element of an instantaneous fault discretized into 1023 elements. Units are those used by Burridge: stress drop = 1, 1 unit of time = time for an S wave to cross one half of the fault. Friction is constant and equal to 0 on the fault plane. The arrows indicate the arrival times of the stopping phases coming from either edge of the fault.

along its entire length and does not propagate. As an example of the numerical accuracy of our BIE method, in Figure 12 we compare the slip velocity as a function of time for the 256-th element of a fault of 1023 elements for the analytical solution (full line) and for the numerical one (dotted line).

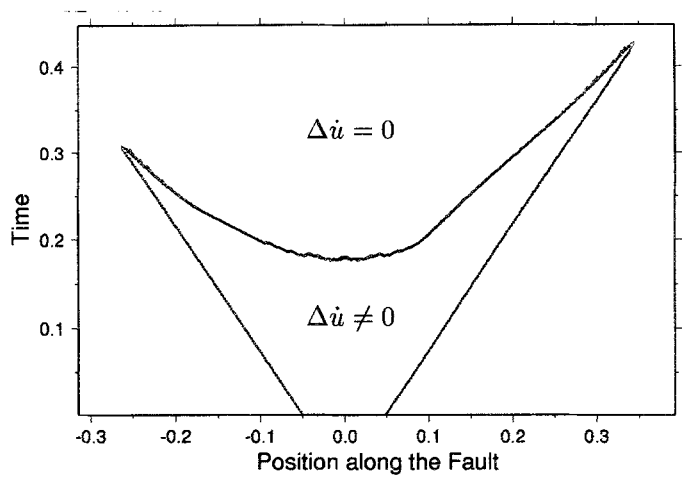

Figure 13

Boundary in the space-time domain between the region where $\Delta\dot{u} \neq 0$ and the one where $\Delta\dot{u} = 0$ in the case of the twin asperity model with rate-dependent friction and propagation at kinematic rupture velocity for the same grid size as in Fig. 9 (dotted line) and for a half as refined grid (diamonds). The rate dependence is $v_0 = 4.5 \times 10^{-2}$ and the rupture fronts propagate kinematically at velocity 0.7β. Space is normalized by the total length of the grid, time is normalized with the time that a shear wave takes to cross this total length.

We see that the numerical solution is very close to the analytical one except near the arrival of the stopping phases coming form the edges of the fault (indicated by arrows).

Study of Convergence of the Numerical Solution for Nonlinear Friction

Figure 13 shows the boundary in the space-time domain of the region where the slip velocity $\Delta\dot{u} \neq 0$ and the one where $\Delta\dot{u} = 0$ in the case of the twin asperity model with rate-dependent friction. Rupture propagation is kinematic with forced rupture velocity equal to 0.7β. Results obtained using the same grid spacing as in Figure 9 are shown with a dotted line. Results obtained using a double-grid spacing are shown with diamonds. The rate dependence is $v_0 = 4.5 \times 10^{-2}$. We observe that the healing

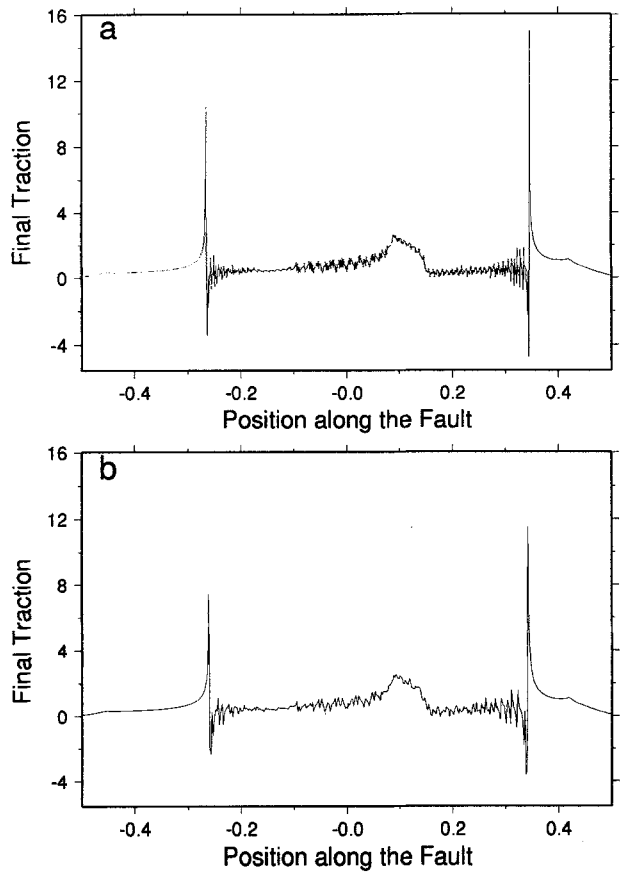

Figure 14

Final traction for the case of the twin asperity model with rate-dependent friction and propagation with fixed rupture velocity. (a) The same grid size as in Figure 9. (b) A grid with half as many points. The rate dependence is $v_0 = 4.5 \times 10^{-2}$ and the rupture fronts propagate kinematically at velocity 0.7β. Space and time are normalized as in Figure 13.

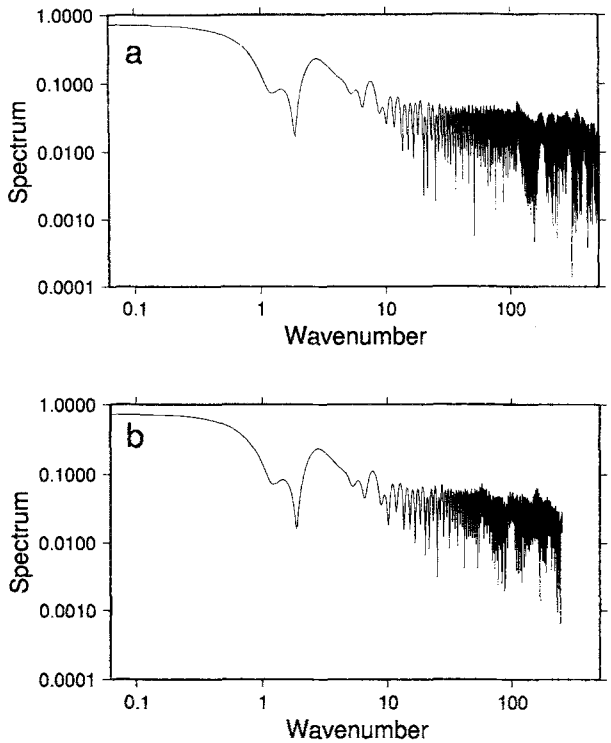

Figure 15

Spectrum of the final traction in the case of the twin asperity model with rate-dependent friction and propagation with fixed rupture velocity. (a) Same grid size as in Fig. 9. (b) A grid with half as many points. The rate dependence is $v_0 = 4.5 \times 10^{-2}$ and the rupture fronts propagate kinematically at velocity 0.7β. Wavenumbers are normalized as in Figure 14 so that 1 corresponds to a wavelength equal to the total size of the grid.

phase describes essentially the same curve in the space time. The abrupt variations near the center of the fault are due to the discrete nature of the calculation. These jumps in healing create the short wavelength noise observed in Figure 14.

Figures 14a and 14b represent the corresponding final tractions for the two different discretizations (the original grid in 14a, the less refined one in 14b).

The maximum traction is higher for the most refined grid because the inverse square root singularity in the region just beyond the crack tip is better resolved. We observe that the low frequencies are preserved in the two cases: in particular the central asperity has the same general shape. The high frequency "noise" can be better analyzed by plotting the spectra of final stress distributions of Figures 14a and 14b on Figures 15a and 15b, respectively.

These figures confirm what could already be seen on Figure 14: low frequencies are well modeled and stable when we change the grid size. The higher wavenumbers, on the other hand, start to diverge beyond nondimensional wavenumbers of

about 50. This corresponds to wavelengths of the order of 0.02 units in Figure 14, which are clearly related to the low amplitude beatings observed inside the fault. These noisy oscillations are due to the interference of the supersonic healing phase with the discrete numerical grid.

Acknowledgements

The present work benefitted from discussions and suggestions from Marc Bonnet, Roland Gaulon, André Herrero, Stefan Nielsen, Dmitri Pisarenko, Stephane Roux, Jean Schmittbuhl and Jean-Pierre Vilotte. We also express thanks to Joe Andrews, Shamita Das and Chris Marone, for their comments and suggestions which helped us to improve the original manuscript.

We gratefully acknowledge the continuous support of our project by the Centre National de Calcul Parallèle en Sciences de la Terre which allowed us to use the CM-5. Invaluable assistance from Patrick Stocklet of this center was essential for overcoming the difficulties of parallel programming on this complex machine.

REFERENCES

AKI, K., and RICHARDS, P. G., *Quantitative Seismology* (New York, Freemann 1980).

BRACE, W. F., and BYERLY, J. D. (1966), *Stick Slip as a Mechanism for Earthquake*, Science *153*, 990–992.

BRUNE, J. N. (1970), *Tectonic Stress and the Spectra of Seismic Shear Waves from Earthquakes*, J. Geophys. Res. *75*, 4997–5009.

BURRIDGE, R. (1969), *The Numerical Solution of Certain Integral Equations with Nonintegrable Kernels Arising in the Theory of Crack Propagation and Elastic Wave Diffraction*, Phil. Trans. R. Soc. A*265*, 363–381.

BURRIDGE, R., and KNOPOFF, L. (1967), *Model and Theoretical Seismicity*, Bull. Seismol. Soc. Am. *57*, 341–371.

CAO, T., and AKI, K. (1986), *Seismicity Simulation with Rate- and State-dependent Friction Law*, Pure Appl. Geophys. *124*, 487–513.

CARLSON, J. M., and LANGER, J. S. (1989), *A Mechanical Model of an Earthquake Fault*, Phys. Rev. A Gen. Phys. *40*, 6470–6484.

COMPTE, D., EISENBERG, A., LORCA, E., PARDO, M., PONCE, L., SARAGONI, R., SINGH, K., and SUÁREZ, G. (1986), *The 1985 Central Chile Earthquake: A Repeat of Previous Great Earthquakes in the Region*?, Science *233*, 449–453.

DAS, S., and AKI, K. (1977a), *A Numerical Study of Two-dimensional Spontaneous Rutpure Propagation*, Geophys. J. R. Astr. Soc. *62*, 591–604.

DAS, S., and AKI, K. (1977b), *Fault Plane with Barriers: A Versatile Earthquake Model*, J. Geophys. Res. *82*, 5658–5670.

DAS, S., and KOSTROV, B. V. (1988), *An Investigation of the Complexity of the Earthquake Source Time Function Using Dynamic Faulting Models*, J. Geophys. Res. *93*, 8035–8050.

DIETERICH, H. (1972), *Time-dependent Friction as a Possible Mechanism for Aftershocks*, J. Geophys. Res. *77*, 3771–3781.

GU, J.-C., RICE, J. R., RUINA, A. R., and TSE, S. (1984), *Slip Motion and Stability of a Single Degree of Freedom Elastic System with Rate- and State-dependent Friction*, J. Mech. Phys. Solids *32*, 167–196.

HEATON, T. H. (1990), *Evidence for and Implications of Self-healing Pulses of Slip in Earthquake Rupture*, Phys. Earth Planet. Int. *64*, 1–20.

KANAMORI, H., and STEWART, G. (1978), *Seismological Aspects of the Guatemala Earthquake of February 4, 1976*, J. Geophys. Res. *83*, 3427–3434.

KOLLER, M., BONNET, M., and MADARIAGA, R. (1992), *Modelling of Dynamical Crack Propagation Using Regularized Time-domain Boundary Integral Equation*, Wave Motion *16*, 339–366.

KORRAT, I., and MADARIAGA, R., *Rupture of the Valparaiso (Chile) Gap from 1971 to 1985.* In *Earthquake Source Mechanics* (eds. Das, S., Boatwright, J., and Scholz, C. H.) (AGU, Washington, DC 1986) pp. 247–258.

KOSTROV, B. V. (1964), *Selfsimilar Problems of Propagation of Shear Cracks*, J. Appl. Math. Mech. *28*, 1077–1087.

KOSTROV, B. V. (1966), *Unsteady Propagation of Longitudinal Shear Cracks*, J. Appl. Math. Mech. *30*, 1241–1248.

MADARIAGA, R. (1979), *On the Relationship between Seismic Moment and Stress Drop in the Presence of Stress and Strength Heterogeneity*, J. Geophys. Res. *84*, 2243–2249.

MADARIAGA, R. (1983), *High Frequency Radiation from Dynamic Earthquake Fault Models*, Annales Geophysicae *1*, 17–23.

MADARIAGA, R., and COCHARD, A. (1992), *Heterogenous Faulting and Friction*, International Symposium on Earthquake Disaster Prevention-Mexico City.

OKUBO, P. (1989), *Dynamic Rupture Modeling with Laboratory-derived Constitutive Relations*, J. Geophys. Res. *94*, 12321–12335.

RICE, J. R. (1993), *Spatio-temporal Complexity of Slip on a Fault*, J. Geophys. Res. *98*, 9885–9907.

RICE, J. R., and RUINA, A. (1983), *Stability of Steady Frictional Slipping*, J. Applied Mech. *50*, 343–349.

SCHWARTZ, D., and COPPERSMITH, K. (1984), *Fault Behaviour and Characteristic Earthquakes: Examples from the Wasacht and San Andreas Fault Zones*, J. Geophys. Res. *89*, 5681–5698.

(Received August 20, 1993, revised February 9, 1994, accepted February 17, 1994)